11-1-2018

Biological effects on uranium isotope fractionation ($^{238}U/^{235}U$) in primary biogenic carbonates

Xinming Chen
School of Earth and Space Exploration

Stephen J. Romaniello
School of Earth and Space Exploration

Achim D. Herrmann
Louisiana State University

Elias Samankassou
Université de Genève

Ariel D. Anbar
School of Earth and Space Exploration

Recommended Citation

Chen, X., Romaniello, S., Herrmann, A., Samankassou, E., & Anbar, A. (2018). Biological effects on uranium isotope fractionation ($^{238}U/^{235}U$) in primary biogenic carbonates. *Geochimica et Cosmochimica Acta, 240*, 1-10. https://doi.org/10.1016/j.gca.2018.08.028

Available online at www.sciencedirect.com

ScienceDirect

Geochimica et Cosmochimica Acta 240 (2018) 1–10

Geochimica et Cosmochimica Acta

www.elsevier.com/locate/gca

Biological effects on uranium isotope fractionation ($^{238}U/^{235}U$) in primary biogenic carbonates

Xinming Chen [a,*], Stephen J. Romaniello [a], Achim D. Herrmann [b], Elias Samankassou [c], Ariel D. Anbar [a,d]

[a] School of Earth and Space Exploration, Arizona State University, Tempe, AZ 85287, USA
[b] Coastal Studies Institute and Department of Geology and Geophysics, Louisiana State University, Baton Rouge, LA 70803, USA
[c] Department of Earth Sciences, University of Geneva, Rue des Maraichers 13, 1205 Geneva, Switzerland
[d] School of Molecular Sciences, Arizona State University, Tempe, AZ 85287, USA

Received 12 May 2018; accepted in revised form 16 August 2018; available online 22 August 2018

Abstract

Determining whether U isotopes are fractionated during incorporation into biogenic carbonates could help to refine the application of $^{238}U/^{235}U$ in $CaCO_3$ as a robust paleoredox proxy. Recent laboratory experiments have demonstrated that heavy uranium (U) isotopes were preferentially incorporated into abiotic aragonite, with an isotope fractionation of ~0.10‰ ($^{238}U/^{235}U$). In contrast, no detectable U isotope fractionation has been observed in most natural primary biogenic carbonates, but the typical measurement precision of these studies was ±0.10‰ and so could not resolve a fractionation of the magnitude observed in the laboratory.

To resolve this issue, we have developed a high precision $^{238}U/^{235}U$ method (±0.02‰, 2 SD) and utilized it to investigate $^{238}U/^{235}U$ in primary biogenic carbonates including scleractinian corals, calcareous green and red algae, echinoderms, and mollusks, as well as ooids from the Bahamas, Gulf of California, and French Polynesia.

Our results reveal that many primary biogenic carbonates indeed fractionate U isotopes during U incorporation, and that this fractionation is in the same direction as observed in abiotic $CaCO_3$ coprecipitation experiments. However, the magnitude of isotope fractionation in biogenic carbonates is often smaller than that predicted by abiotic $CaCO_3$ coprecipitation experiments (0.00–0.09‰ vs. 0.11 ± 0.02‰), suggesting that one or more processes suppress U isotope fractionation during U incorporation into biogenic carbonates. We propose that closed-system behavior due to the isolation of the local calcification sites from ambient seawater, and/or kinetic/disequilibrium isotope fractionation caused by carbonate growth kinetics, explains this observation. Our results indicate that U isotope fractionation between biogenic carbonates and seawater might help to constrain U partition coefficients, carbonate growth rates, or seawater chemistry during coprecipitation.

Keywords: Primary carbonates; Biological effects; $^{238}U/^{235}U$; The Bahamas

1. INTRODUCTION

Because of the relatively long residence time of uranium (U) in the oceans (~500 kyr; Dunk et al., 2002), the wide spatial-temporal distribution of sedimentary carbonate rocks in geologic record (Mackenzie and Morse, 1992; Shields and Veizer, 2002), and the fractionation of U isotopes during removal into anoxic sedimentary environments, the measurement of variations of $^{238}U/^{235}U$ in marine carbonates is finding application as a promising proxy to reconstruct global redox conditions of oceans

* Correspondence author.
E-mail address: xchen147@asu.edu (X. Chen).

https://doi.org/10.1016/j.gca.2018.08.028
0016-7037/

through time (Brennecka et al., 2011; Dahl et al., 2014, 2017; Lau et al., 2016, 2017; Elrick et al., 2017; Jost et al., 2017; Song et al., 2017; Bartlett et al., 2018; Clarkson et al., 2018; Zhang et al., 2018a,b). Early efforts to develop this proxy assumed that marine carbonates directly record seawater $^{238}U/^{235}U$ (e.g., Brennecka et al., 2011). However, there is a risk that abiotic and/or biological processes fractionate U isotopes during incorporation into biogenic precipitates as is observed for other isotopes systems (e.g., $\delta^{53}Cr$ and $\delta^{11}B$; Henehan et al., 2016; Wang et al., 2016). If there were U isotope fractionation in these processes, $^{238}U/^{235}U$ in sedimentary carbonates would fail to faithfully record that of seawater, and significantly affect the reconstruction of paleoredox conditions. For example, an isotope fraction of 0.10‰ for $^{238}U/^{235}U$ during U incorporation into calcium carbonates corresponds to an offset of 18% in the inferred extent of oceanic anoxia (Chen et al., 2017). Thus, it is essential to examine the U isotope fractionation during U incorporation into biogenic carbonates.

To address this issue, several previous studies examined $^{238}U/^{235}U$ variations in biogenic carbonates including corals, calcareous green and red algae, and mollusks and found that $^{238}U/^{235}U$ ratios were statistically indistinguishable from modern seawater at a typical measurement precisions of ±0.10‰ (2 SD; Stirling et al., 2007; Weyer et al., 2008; Romaniello et al., 2013). A few higher precision measurements of fossil coral samples reached a similar conclusion at precision of approximately ±0.03‰ (2 SD; Andersen et al., 2010). However, abiotic $CaCO_3$ coprecipitation experiments demonstrated measurable U isotope fractionation (~0.10‰) during U incorporation into carbonates at pH ~8.5, with heavier U isotopes preferentially enriched in precipitates (Chen et al., 2016). Based on these experiments, Chen et al. (2017) predicted that the isotope fractionation between modern seawater and abiotic carbonates should be $\sim 0.11 \pm 0.02$‰. However, this estimate is inconsistent with available evidence that suggests no apparent fractionation in biogenic carbonates. This inconsistency suggests that either the current the precision of U isotope measurement have not been able to resolve the U isotope fractionation in biogenic carbonates, or that biogenic carbonates display so called 'vital effects' which cause U to fractionate differently when partitioning into biogenic and abiogenic carbonates. Clarifying this issue has important implications for both understanding the mechanisms of U incorporation into biogenic carbonates and improving the U isotope paleoredox proxy. To this end, we developed a new method for high precision measurement of $^{238}U/^{235}U$ and applied this method to measure $^{238}U/^{235}U$ in a variety of primary biogenic carbonates.

2. SAMPLES

We measured a variety of primary biogenic carbonates samples including several species of scleractinian corals, calcareous green and red algae, mollusks and echinoderms (Table 1). Specimens were mainly collected from the the pertidal and subtidal zones of the Exumas region of the Bahamas at the Little Darby Research Station and were previously described by Romaniello et al. (2013). Individual hand samples were collected from the sediment surface. When necessary, multiple specimens from the same sample location were pooled to provide sufficient U for high precision U isotope analyses. Ooid sands, which cover hundreds of square kilometers on the Bahamas platform (Harris, 2010), were sieved to purify ooids from the remaining detritus. Two additional coral samples from French Polynesia (Pretet et al., 2013) and one mollusk specimen from the Gulf of California are also included. All these biogenic carbonate precipitates are aragonite, except the red algae (high-magnesium calcite) and echinoderms (calcite, Romaniello et al., 2013).

3. HIGH PRECISION $^{238}U/^{235}U$ MEASUREMENT

U isotopic ratios ($^{238}U/^{235}U$ and $^{234}U/^{238}U$) were measured on a multiple collector inductively coupled plasma mass spectrometer (MC-ICP-MS) using the ^{233}U-^{236}U double-spike method (Weyer et al., 2008; Chen et al., 2016). To increase the precision of the measurement of $^{238}U/^{235}U$ compared to prior studies, we analyzed sample solutions at a concentration of 200 ppb as compared to the more typical 50 ppb. To this end, we reconfigured the mass spectrometer with 10^{10} Ω and 10^{12} Ω resistors on particular Faraday collectors, as described below. We also describe below some modifications of the sample preparation and U purification procedures necessitated by these larger sample sizes.

3.1. Sample preparation

Primary biogenic carbonate precipitates were cleaned using Milli-Q water (18.2 MΩ) and dried at 105 °C for 48 h. Dried samples were powdered in a ball mill equipped with trace-metal-clean silicon carbide mortars. To acquire the bulk U concentration and isotopic compositions of these biogenic carbonates samples, chunks of ~15 g of corals and red algae, and the whole mollusks, green algae, and echinoderms were powdered for chemical analysis.

Carbonate samples (0.5–10 g) were dissolved in excess 1 M HNO_3 (all the reagents used are trace-metal grade) overnight and centrifuged at a rate of 4500 rpm to remove any insoluble material. A 50 μL aliquot of clear supernatant was used for analysis of major cations and trace metal concentrations on a Thermo iCAP Q ICP-MS at ASU. Samples were spiked with a ^{233}U-^{236}U double-spike (IRMM-3636) at a 0.0363 spike:sample molar ratio (Verbruggen et al., 2008; Chen et al., 2016). The spiked samples were then dried down completely and digested with concentrated HNO_3 + 30% H_2O_2 repeatedly to remove any residual organic matter. The digested samples were finally dissolved in 3 M HNO_3 in preparation for column chemistry. To avoid high concentrations of Ca^{2+} and SO_4^{2-}, which spontaneously nucleate and precipitate as $CaSO_4$ on the UTEVA resin, the Ca concentration was kept under 20 mg/ml in the loading acid.

Table 1
Sample information, U concentration, $\delta^{234}U$, and $\delta^{238}U$ for modern carbonate samples.

				Romaniello et al. (2013)			This study			
Samples	Species	Locations	Carbonate mineralogy	$\delta^{238}U$‰	2 SE‰	N	U ppm	$\delta^{238}U$‰	2 SE‰	N
Coral	*Diploria strigose*	Bahamas	Aragonite	−0.39	0.08	3	2.56	−0.37	0.01	16
Coral	*Siderastrea radians*	Bahamas	Aragonite	−0.37	0.08	3	2.6	−0.37	0.01	8
Coral	*Porites divaricata*	Bahamas	Aragonite	−0.37	0.09	3	2.61	−0.37	0.02	8
Coral	*Porites asteroides*	Bahamas	Aragonite	−0.37	0.09	3	2.86	−0.37	0.02	8
Coral	*Porites spirobranchus*	French Polynesia	Aragonite	–	–	–	2.32	−0.38	0.02	8
Coral	*Porites spirobranchus*	French Polynesia	Aragonite	–	–	–	2.11	−0.37	0.02	8
Mollusks	*Tellina listeri* (dead)	Bahamas	Aragonite	−0.38	0.08	3	0.06	−0.40	0.02	3
Mollusks	*Modiolus capax* (dead)	Gulf of California	Aragonite	–	–	–	0.06	−0.31	0.02	3
Green algae	*Acetabularia crenulata* (head, live)	Bahamas	Aragonite	−0.36	0.06	3	0.58	−0.33	0.02	3
Green algae	*Acetabularia crenulate* (stalk, live)	Bahamas	Aragonite	−0.34	0.09	3	1.05	−0.36	0.02	4
Green algae	*Rhipocephalus phoenix* (stalk, live)	Bahamas	Aragonite	−0.41	0.06	3	2.22	−0.34	0.01	8
Green algae	*Rhipocephalus phoenix* (leaves, live)	Bahamas	Aragonite	−0.42	0.09	3	1.65	−0.37	0.01	5
Green algae	*Halimeda incrassate* (whole, live)	Bahamas	Aragonite	–	–	–	1.25	−0.36	0.02	6
Green algae	*Penicillus capitatus* (head, live)	Bahamas	Aragonite	−0.43	0.07	3	1.95	−0.34	0.02	7
Green algae	*Penicillus capitatus* (stalk, live)	Bahamas	Aragonite	−0.25	0.06	3	1.33	−0.38	0.01	5
Red algae	*Neogoniolithon strictum* (live)	Bahamas	High-Mg calcite	−0.44	0.06	3	0.68	−0.35	0.02	7
Echinoderm	*Clypeaster subdepressus* (dead)	Bahamas	Calcite[a]	–	–	–	0.26	−0.30	0.02	4
Ooids	–	Bahamas	Aragonite	−0.27	0.07	3	2.85	−0.24	0.02	7
Seawater	–	Bahamas	–	–	–	–	0.003	−0.39	0.02	3

Note: N represents the number of measurements for each sample on the MC-ICP-MS. $\delta^{238}U$ is the average value of multiple measurements.
[a] Gilbert and Wilt (2011).

3.2. U purification

We used a slightly modified purification protocol to accommodate the larger sample sizes required for high-precision analyses. Briefly, after rinsing the polypropylene columns with 18.2 MΩ cm deionized water, ~1 ml UTEVA resin (Eichrom Technologies, LLC) was loaded into 10 mL chromatography columns (Bio-Rad Laboratories, Inc.). The resin was cleaned with 4 × 2.5 ml 0.05 M HCl to remove any trace U introduced during the loading step. Following this, the resin was washed with 3 × 1 ml 3 M HNO_3 to convert it to the nitrate form. Samples were loaded onto the columns in approximately 50 ml of 3 M HNO_3. To completely remove all the matrix ions except U and Th, an extended elution consisting of ~15 ml of 3 M HNO_3 (loaded in 1 + 2 + 3 + 4 + 5 mL aliquots) was used to rinse the resin. The remaining steps used to elute Th and U were identical to those reported in Chen et al. (2016). This UTEVA column protocol was repeated a second time to further purify U in order to ensure high-precision isotopic analyses. Following column chemistry, the U-containing eluent was dried down and digested with concentrated HNO_3 + 30% H_2O_2 several times to remove trace organic contamination from the resin.

3.3. U isotope analysis

In order to obtain higher analytical precision, we increased the U concentration and beam intensity used during analysis, while accommodating the high dynamic range of $^{238}U/^{235}U$ ratios by using a 10^{10} Ω resistor on the Faraday collector assigned to ^{238}U and three 10^{12} Ω resistors on the collector for ^{233}U, ^{235}U, and ^{236}U. ^{234}U was measured using a 10^{11} Ω resistor. We tested analyses at a series of increasing U concentrations (50, 100, 200, and 400 ppb), which were all introduced using a 50 μL min^{-1} PFA nebulizer and Apex-Q desolvation system (Elemental Scientific, Inc) and a combination of "Jet" sample cone and normal "H" skimmer cone (Thermo Fisher Scientific, Inc.). Under these conditions, signal intensity increased linearly with concentration, and measurement voltages for ^{235}U and ^{238}U were about 0.88 V and 120 V, respectively, when using a 200 ppb U solution. Each measurement consisted of a 110 s uptake time, 50 cycles (8.4 s per cycle), and a 210 s washout time. Samples analyses were bracketed by analyses of identically double-spiked CRM145a standard every 2 analyses in order to account for any non-ideal behavior of the double-spike correction due to peak tailing and deviation from a pure exponential law mass bias in the ICP-MS interface as previously reported (Chen et al., 2016).

U isotopic composition is reported in δ notation relative to the standard CRM-145a using the following equation:

$$\delta^{238}U = \left[\frac{(^{238}U/^{235}U)_{sample}}{(^{238}U/^{235}U)_{CRM-145a}} - 1\right] \times 1000 \quad (1)$$

where the subscripts 'sample' and 'CRM-145a' stand for sample and the U reference standard CRM-145a. To obtain lower uncertainty in $\delta^{238}U$, we measured each carbonate sample ~8 times following U purification. The uncertainty of the U isotopic compositions in samples was reported as two standard error of the mean (2 SE). For these high precision measurements, we prefer to report the standard error of the mean rather than the more commonly used standard deviation in order to recognize the additional precision obtained through repeated analyses of samples solutions following column chemistry.

4. RESULTS

4.1. Precision and accuracy of $\delta^{238}U$ analysis

The precision obtained for both $\delta^{238}U$ and $\delta^{234}U$ increase with U concentration (Fig. 1). The observed improvement in measurement precision is consistent with errors predicted from the combined consideration of counting errors, thermal noise, and electronic noise in the amplifier circuits (John and Adkins, 2010).

Considering the sample size required for U isotopic measurement and significant improvement of the measurement precision for $\delta^{238}U$ at higher U concentrations, we chose to analyze natural carbonate samples at a U concentration of 200 ppb, which allows ~8 analyses of typical 1 g carbonate sample containing ~1.6 μg of U. The typical precision achieved for $\delta^{238}U$ measurements in natural carbonate samples (±0.03–0.05‰, 2 SD) is slightly worse than achieved for the pure CRM-145a reference standard (±0.02‰). Subsequent method development suggests that this might have been due to small amounts of Na which is often leached from the UTEVA resin during sample purification.

The blank from the U purification procedure was about 0.09 ± 0.05 ng (2 SD, N = 6, see Table S3), which was negligible compared to the amount of U used in each sample (>600 ng). Six aliquots of the pure CRM-145a were processed through the UTEVA column chemistry together with natural biogenic carbonate samples and acquired an average $\delta^{238}U$ value of 0.00 ± 0.03‰ (2 SD, N = 6, see Table S3), which was the same as the direct measurement of pure CRM-145a (0.00 ± 0.03‰).

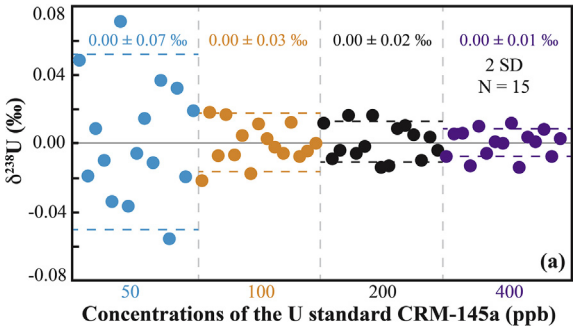

Fig. 1. $\delta^{238}U$ of CRM-145a measured at U concentrations of 50, 100, 200 and 400 ppb. The horizontal solid line represents the overall average values of $\delta^{238}U$. The horizontal dashed lines represent theoretically predicted 2 SD uncertainty for $\delta^{238}U$ based on counting errors, thermal noise, and electronic noise in the amplifiers (e.g., John and Adkins, 2010).

Supplementary data associated with this article can be found, in the online version, at https://doi.org/10.1016/j.gca.2018.08.028.

4.2. U concentration in carbonates

U concentration varies significantly among different types of primary biogenic carbonates, in the descending order of scleractinian corals (2.11–2.86 ppm), calcareous red and green algae (0.58–2.22 ppm), echinoderm (0.26 ppm) and mollusks (0.06 ppm, Table 1 and Fig. 2b). The ooids in this study had a U concentration of 2.85 ppm.

4.3. $\delta^{238}U$ in carbonates

In contrast with previous measurements, our new high precision measurements of $\delta^{238}U$ demonstrate that many primary biogenic carbonates show small, but clearly resolved, isotope fractionation from seawater. Compared to the average $\delta^{238}U$ of modern seawater, $-0.39 \pm 0.01‰$ (Tissot and Dauphas, 2015; this study), our samples display fractionation over a range of 0.00–0.09‰, with the carbonate phase enriched in ^{238}U (Fig. 2c). Corals, algae, and all primary biogenic carbonates display $\delta^{238}U$ significantly heavier than seawater (Student's t-test, $p < 0.05$, Tables S-1 and S-2). $\delta^{238}U$ in scleractinian corals from the Bahamas and French Polynesia are the same with an average value of $-0.37 \pm 0.01‰$ (2 SE, number of coral samples, N = 6). In contrast, $\delta^{238}U$ values in mollusks are most likely species-dependent. Although *Tellina listeri* and *Modiolus capax* shared the same U concentration (0.06 ppm), $\delta^{238}U$ in the latter ($-0.31 \pm 0.02‰$, 2 SE) is heavier than the former ($-0.40 \pm 0.02‰$, 2 SE). Similarly, green and red algae fractionate U isotopes by about 0.01–0.06‰. The echinoderm sand dollar specimen (*Clypeaster subdepressus*) displayed the largest isotopic offset, ~0.09‰. $\delta^{238}U$ of the ooids is 0.15‰ heavier than modern seawater.

5. DISCUSSION

5.1. U isotope fractionation in primary biogenic carbonates

High-precision measurements of $^{238}U/^{235}U$ variations in biogenic carbonates reveal a range of U isotope fractionation in these samples with values typically 0.00–0.09‰ heavier than coeval seawater. To interpret the observed range of variation for U isotopes recorded in biogenic carbonates, we propose two hypotheses: (1) equilibrium isotope fractionation occurs at calcification sites with varying degrees of restriction from seawater; or (2) kinetic/disequilibrium isotope fractionation is caused by rapid $CaCO_3$ precipitation at calcification sites. These hypotheses are discussed in more detail below.

5.1.1. Semi-restricted equilibrium isotope fractionation model

One possible explanation for the variation in isotopic fractionation we observed between different biogenic carbonates is that the intrinsic equilibrium fractionation of U isotopes in primary biogenic carbonates is similar to that observed in abiotic $CaCO_3$ coprecipitation experiments, but that the magnitude of the isotope fractionation depends on the extent of the isolation of the local calcification sites from ambient seawater (Fig. 3; Chen et al., 2016). Previous abiotic $CaCO_3$ coprecipitation experiments demonstrated an equilibrium isotope fractionation of 0.00–0.10‰. This fractionation was interpreted to be dependent on the aqueous speciation of U, which in turn depends on Ca^{2+} and Mg^{2+} concentrations, alkalinity, pCO_2, pH and ionic strength (Chen et al., 2016). Based on this work, the U isotope fractionation during coprecipitation of U with abiotic

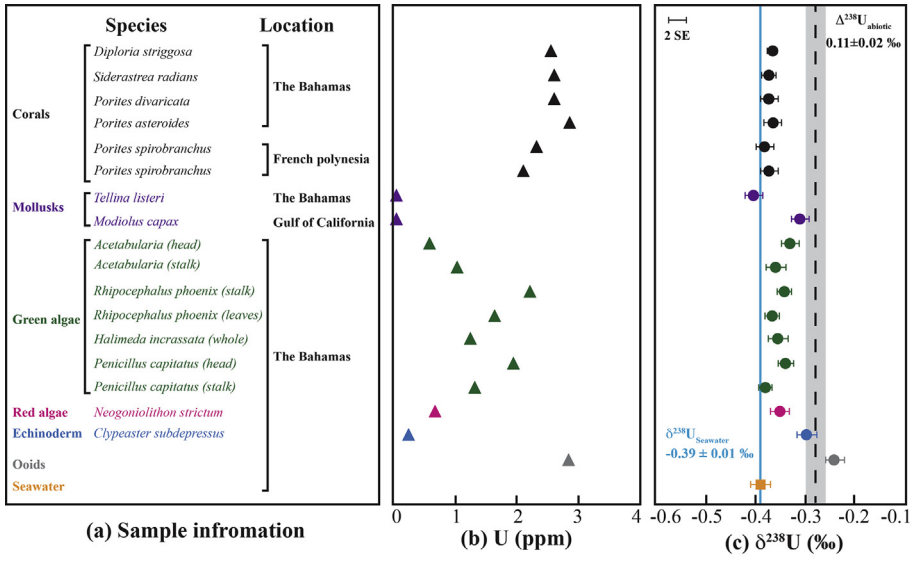

Fig. 2. Sample information (a), U concentration (b), and $\delta^{238}U$ (c) in modern carbonates. The blue solid lines in panels (c) represents $\delta^{238}U$ in modern seawater (Tissot and Dauphas, 2015; this study). The gray band in panel (c) stands for the predicted range of $\delta^{238}U$ in abiotic carbonates in equilibrium with modern seawater ($\Delta^{238}U_{abiotic} = 0.11 \pm 0.02‰$; Chen et al., 2016). (For interpretation of the references to colour in this figure legend, the reader is referred to the web version of this article.)

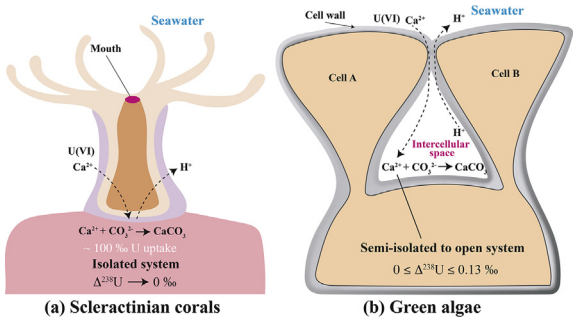

Fig. 3. Schematic illustration of U uptake and isotope fractionation in (a) scleractinian corals and (b) green algae (modified from Adey and Loveland, 2007; Galloway et al., 2007).

calcite and aragonite in modern seawater was predicted to be 0.11 ± 0.02‰ (Chen et al., 2017). If the calcification sites of primary biogenic carbonates are fully open to exchange with seawater and coprecipitation took place at isotopic equilibrium, we would expect to see an isotope fractionation of 0.11 ± 0.02‰ (Chen et al., 2016, 2017). On the other hand, increasing restriction of calcification sites should lead to more closed system behavior which reduces the apparent isotope fractionation factor due to mass balance. In the end-member case, where calcification sites are completely isolated from the ambient seawater, nearly quantitative U removal from the calcifying fluid will result in no isotope fractionation from seawater.

Here, we applied a Rayleigh fractionation model to examine the U isotope fractionation in scleractinian corals and calcareous green algae. Experimental studies demonstrated direct and rapid transport of the surrounding seawater to the coral calcification sites, which are mostly isolated from ambient seawater (Fig. 3a; Gagnon et al., 2007, 2012; Tambutté et al., 2012). Elevation of pH by ~1 unit at the local calcification sites leads to rapid precipitation of $CaCO_3$, leading to almost 100% incorporation of U into carbonates (Al-Horani et al., 2003; Gaetani et al., 2011). This is in agreement with our observation that the $^{238}U/^{235}U$ of corals is very close to that of the ambient seawater.

The variable U isotope fractionation in green algae might result from variable isolation of the calcification sites during different growth stages of the organism. $CaCO_3$ precipitates in the intercellular spaces of green algae (Fig. 3b; Adey and Loveland, 2007). At the early growth stage of green algae cells, the intercellular spaces are open to seawater, resulting in an open-system Rayleigh isotope fractionation similar to abiotic $CaCO_3$ precipitates in seawater (0.11 ± 0.02‰; Chen et al., 2017). However, as the walls of the adjacent cells grow together, the intercellular space becomes increasingly isolated from ambient seawater (Fig. 3b; Adey and Loveland, 2007). Once completely isolated, U inside the intercellular spaces will be 100% incorporated into carbonate precipitates in green algae, directly recording $^{238}U/^{235}U$ of the ambient seawater. Incorporation of U into green algae cells at different growth stages can therefore explain variable U isotope fractionation in these species, and even variable isotope fractionation between different parts of the same individual (e.g., stalk and head). Similar to green algae, calcification process occurs in the intercellular spaces in red algae (Krumbein, 1979), suggesting that the semi-restrict equilibrium isotope fractionation model could also interpret the U isotope fractionation observed in red algae.

Although the specific mechanisms of U incorporation into mollusks and echinoderms are not well understood, Ca uptake by these organisms suggests that U isotope fractionation might be governed by U transport processes within mollusks and echinoderms in addition to the extent of isolation of the calcification site from ambient seawater. For example, experiments using ^{45}Ca radiotracer demonstrated that mollusks adsorb dissolved Ca^{2+} from ambient seawater via the epithelial cells of the gill, inner mantle, and digestive canal. Ca is then delivered by the body fluids to the extrapallial space, which is isolated from ambient seawater, for calcification (Jodrey, 1953). If U were incorporated into mollusks in the same way as Ca, U isotope fractionation in the shells of mollusks would be controlled by U transport processes and the extent of the isolation of the calcification site. Similar to mollusks, the formation of skeletons of echinoderms is also a biologically controlled intracellular biomineralization process (Nakano et al., 1963; Gorzelak et al., 2011). Thus, variations in $\delta^{238}U$ of the shells of mollusks and echinoderms likely result from the biologically controlled U transport processes and the isolation of the calcification site from ambient seawater.

5.1.2. Kinetic/disequilibrium isotope fractionation model

An alternative explanation for the variation in U isotope fractionation observed between different primary biogenic carbonates is that U isotopic fractionation is controlled by differences in kinetic/disequilibrium isotopic effects resulting from differences in the $CaCO_3$ precipitation rates. The U isotope fractionation ($\Delta^{238}U_{biogenic}$) between primary biogenic carbonates (except one mollusk sample) and seawater appears to decrease with the U partition coefficients (K_d) in $CaCO_3$ (Fig. 4a). The U partition coefficient K_d is defined as:

$$K_d = \frac{([U]/[Ca])_{CaCO_3}}{([U]/[Ca])_{aqueous}} \quad (2)$$

where $([U]/[Ca])_{CaCO3}$ and $([U]/[Ca])_{aqueous}$ are the molar concentration ratios of U to Ca in the bulk $CaCO_3$ and the aqueous solution, respectively (Curti, 1999).

U isotope fractionation in laboratory-synthesized abiotic aragonite also showed a decreasing U isotope fractionation with increasing partition coefficient of U, suggesting that biogenic carbonates might fractionate U isotopes in the same way as abiotic aragonite (Fig. 4b and Table 2; Chen et al., 2016). In abiotic aragonite coprecipitation experiments, K_d of U increased with aragonite growth rate (Fig. 4c; Gabitov et al., 2008; Chen et al., 2016), resulting in an overall trend toward smaller U isotope fractionation with increasing precipitation rate (Fig. 4d). One possible explanation for this pattern is that at high precipitation rates, U is less selectively incorporated into the rapidly growing carbonate lattice, while at slower precipitation rates, incorporation of various aqueous U species is more

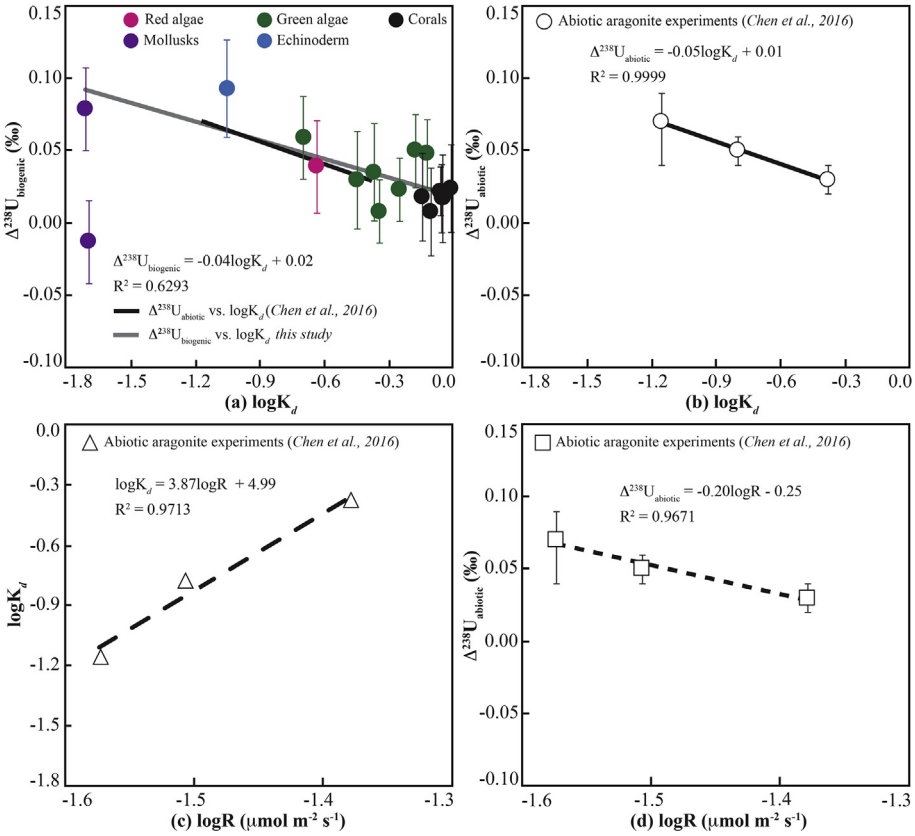

Fig. 4. U isotope fractionation during U incorporation into (a) primary biogenic carbonates ($\Delta^{238}U_{biogenic}$; this study, 2 SE) and (b) abiotic aragonite ($\Delta^{238}U_{abiotic}$; Chen et al., 2016) versus U partition coefficient logK_d (Fig. S1) (c) U partition coefficient logK_d in abiotic aragonite versus growth rate logR. (d) $\Delta^{238}U_{abiotic}$ versus abiotic aragonite growth rate logR (see Supplementary material). The black solid lines in (a) and (b) represent the linear regression of $\Delta^{238}U_{abiotic}$ over logK_d observed in abiotic aragonite coprecipitation experiments (Chen et al., 2016). The gray solid line in (a) is the linear regression of $\Delta^{238}U_{biogenic}$ vs. logK_d, excluding one mollusk sample ($\delta^{238}U = -0.40‰$). The black dashed lines in (c) and (d) are the linear regressions of logK_d and $\Delta^{238}U_{abiotic}$ over logR.

Table 2
Summary of U partition coefficients, carbonate growth rates and U isotope fractionation in abiotic aragonite coprecipitation experiments.

Aragonite experiments	$f_{neutral}$	K_d	logK_d	R mmol m^{-2} s^{-1}	logR mmol m^{-2} s^{-1}	$\Delta^{238}U_{abiotic}$‰
A1	0.27	0.07	−1.15	0.0267	−1.57	0.07 + 0.02/−0.03
A1*	0.24	0.17	−0.77	0.0311	−1.51	0.05 + 0.01/−0.01
A3	0.13	0.42	−0.38	0.0418	−1.38	0.03 + 0.01/−0.01

Note: $f_{neutral}$ is the fraction of the neutral U species $Ca_2UO_2(CO_3)_3(aq)$. R is the aragonite growth rate (see Supplementary material). All these data were from previous abiotic aragonite coprecipitation experiments (Chen et al., 2016).

selective leading to the preferential incorporation of one or more isotopically heavy U species.

Likewise, differences in biogenic carbonate precipitation rates might also lead to variations in $\Delta^{238}U_{biogenic}$. The $CaCO_3$ precipitation rate of corals typically ranges from 2.5 to 6.9 μmol m^{-2} s^{-1}, which is much faster than that observed for the green and red algae (0.001–0.74 μmol m^{-2} s^{-1}; Wray, 1977; Gattuso et al., 1993, 1996; Ohde and van Woesik, 1999; Bates et al., 2001; Ortegón-Aznar et al., 2017). Although areal calcification rates are unavailable for mollusks and echinoderms, the close correlation between the apparent K_d and U isotope fractionation in biogenic carbonates suggest that a similar process might explain the range of observed values.

We are unaware of any dedicated biotic experiments designed to test the effect of varying carbonate precipitation rate on U isotope fractionation during U coprecipitation with calcite or aragonite, but our observations above suggest that such work might be warranted.

5.2. U isotope fractionation in ooids

The U isotope fractionation observed in ooids is uniquely significant because the formation of these

precipitates most closely resembles the processes occurring in abiotic aragonite coprecipitation experiments (Chen et al., 2016). While the formation of ooids is microbially meditated through prenucleation of amorphous calcium carbonate that transforms into aragonite in the ambient seawater (Diaz et al., 2014, 2015, 2017), this process most likely is continuous and in direct contact with ambient seawater. Radiocarbon ages for the innermost and outermost cortices of Bahamian ooids suggest that formation probably occurs episodically over a period of hundreds to thousands of years (Duguid et al., 2010). The magnitude of U isotope fractionation ($\Delta^{238}U$) in the ooid samples ($0.15 \pm 0.02‰$) is close to the U isotope fractionation predicted for the abiotic coprecipitation of U with $CaCO_3$ in modern seawater ($0.11 \pm 0.02‰$, Chen et al., 2016, 2017), which provides empirical support for the speciation-controlled isotopic fractionation model of Chen et al. (2016), although we cannot definitely rule out a kinetic origin for the observed isotope fractionation as discussed above.

5.3. Implications for U incorporation into biogenic carbonates

The magnitude of U isotopic fractionation during U coprecipitation into biogenic carbonates might provide novel constraints on the processes controlling U/Ca partitioning in various biogenic carbonates. The U/Ca ratio in biogenic carbonates such as corals has been suggested as a proxy for reconstructing paleoclimate conditions because of its strong correlations with seawater temperature, pH, or CO_3^{2-} concentration (Min et al., 1995; Shen and Dunbar, 1995; Felis et al., 2009; Armid et al., 2011; Anagnostou et al., 2011; Inoue et al., 2011). However, the exact factors which predominantly control U/Ca ratios in biogenic carbonates remain a matter of debate.

The negative correlation between U isotope fractionation and both the U distribution coefficient and carbonate growth rate might provide clues to answer this question. Uranium isotopes likely provide a unique probe of aqueous U speciation at the calcification site, which reflects a complex interplay between pH and CO_3^{2-} concentrations in the calcifying fluids as well as factors like restriction of the calcification site from seawater and the local calcification rate (e.g., Keul et al., 2013; Endrizzi and Rao, 2014; DeCarlo et al., 2015). For example, the elevations in pH, Ca^{2+}, and CO_3^{2-} concentrations at the calcification sites of corals significantly increased the supersaturation of aragonite, to 6 times that of seawater and changed aqueous U speciation (Al-Horani et al., 2003; Chen et al., 2016). Similarly, calcareous green algae also have isolated calcification sites between two cells that increased $CaCO_3$ supersaturation (Borowitzka, 1982; Adey and Loveland, 2007; Wizemann et al., 2014). These isolated calcification sites significantly increased the carbonate growth rate and elevated the partition coefficient of U in biogenic carbonates (Gabitov et al., 2008; Chen et al., 2016). Although our understanding of how these processes impact U isotope fractionation is admittedly in its infancy, future work combining studies of partition coefficients and U isotope fractionation during U coprecipitation in biogenic carbonates might offer better constraints than have been available from U/Ca ratios alone.

6. CONCLUSIONS

High precision measurements of $\delta^{238}U$ demonstrate small but resolvable U isotope fractionation (0.00–0.09‰) during U incorporation into primary biogenic carbonates. The magnitude of U isotope fractionation in these biogenic carbonates is similar to or smaller than previously reported abiotic aragonite coprecipitation experiments. Variations of $\delta^{238}U$ in different primary biogenic carbonates likely depend on either the extent of the isolation of the calcification sites from ambient seawater or calcium carbonate growth rates. In additional, U isotope fractionation during coprecipitation may eventually prove to be useful probe of aqueous U speciation in seawater and/or local calcifying fluids.

ACKNOWLEDGEMENTS

This work was supported by the U.S. National Science Foundation (Grant OCE-0952394) and the NASA Exobiology Program. The authors would like to acknowledge and thank Adam Turner, Dr. Gregory Brennecka, and Dr. Dawn Summer who helped us collect the biogenic carbonate samples for this work, as well as Dr. Pamela Reid and the entire staff of the Darby Island Research Station who provided both their scientific support and generous hospitality during field work for this project. We thank the reviewer Ashleigh van Smeerdijk Hood and the other two anonymous reviewers for suggestions that improved the manuscript.

REFERENCES

Adey W. H. and Loveland K. (2007) Biomineralization and calcification: a key to biosphere and ecosystem function. In *Dynamic Aquaria: Building and Restoring Living Ecosystems*, third ed. Academic Press, London, pp. 145–147.

Al-Horani F. A., Al-Moghrabi S. M. and de Beer D. (2003) The mechanism of calcification and its relation to photosynthesis and respiration in the scleractinian coral *Galaxea fascicularis*. *Mar. Biol.* **142**, 419–426.

Anagnostou E., Sherrell R. M., Gagnon A., LaVigne M., Field M. P. and McDonough W. F. (2011) Seawater nutrient and carbonate ion concentrations recorded as P/Ca, Ba/Ca, and U/Ca in the deep-sea coral *Desmophyllum dianthus*. *Geochim. Cosmochim. Acta* **75**, 2529–2543.

Andersen M. B., Stirling C. H., Zimmermann B. and Halliday A. N. (2010) Precision determination of the open ocean $^{234}U/^{238}U$ composition. *Geochem. Geophys. Geosyst.* **11**, Q12003. https://doi.org/10.1029/2010GC003318.

Armid A., Asami R., Fahmitati T., Sheikh M. A., Fujimura H., Higuchi T., Taria E., Shinjo R. and Oomori T. (2011) Seawater temperature proxies based on D_{Sr}, D_{Mg}, and D_U from culture experiments using the branching coral *Porites cylindrical*. *Geochim. Cosmochim. Acta* **75**, 4273–4285.

Bartlett R., Elrick M., Wheeley J. R., Polyak V., Desrochers A. and Asmerom Y. (2018) Abrupt global-ocean anoxia during the Late Ordovician-early Silurian detected using uranium isotopes of marine carbonates. *Proc. Natl. Acad. Sci.* **115**, 5896–5901.

Bates N. R., Samuels L. and Merlivat L. (2001) Biogeochemical and physical factors influencing seawater fCO_2 and air-sea CO_2

exchange on the Bermuda coral reef. *Limnol. Oceanogr.* **46**, 833–846.

Borowitzka M. A. (1982) *Mechanisms in algal calcification*. Elsevier Biomedical Press B.V., pp. 138–177.

Brennecka G. A., Herrmann A. D., Algeo T. J. and Anbar A. D. (2011) Rapid expansion of oceanic anoxia immediately before the end-Permian mass extinction. *Proc. Natl. Acad. Sci.* **108**, 17631–17634.

Chen X., Romaniello S. J., Herrmann A. D., Wasylenki L. E. and Anbar A. D. (2016) Uranium isotope fractionation during coprecipitation with aragonite and calcite. *Geochim. Cosmochim. Acta* **188**, 189–207.

Chen X., Romaniello S. J. and Anbar A. D. (2017) Uranium isotope fractionation induced by aqueous speciation: implications for U isotopes in marine $CaCO_3$ as a paleoredox proxy. *Geochim. Cosmochim. Acta* **215**, 162–172.

Clarkson M. O., Stirling C. H., Jenkyns H. C., Dickson A. J., Porcelli D., Moy C. M., von Strandmann P. A. E. P., Cooke I. R. and Lenton T. M. (2018) Uranium isotope evidence for two episodes of deoxygenation during Oceanic Anoxic Event 2. *Proc. Natl. Acad. Sci.* **108**, 17631–17634.

Curti E. (1999) Coprecipitation of radionuclides with calcite: estimation of partition coefficients based on a review of laboratory investigations and geochemical data. *Appl. Geochem.* **14**, 433–445.

Dahl T. W., Boyle R. A., Canfield D. E., Connelly J. N., Gill B. C., Lenton T. M. and Bizzarro M. (2014) Uranium isotopes distinguish two geochemically distinct stages during the later Cambrian SPICE event. *Earth Planet. Sci. Lett.* **401**, 313–326.

Dahl T. W., Connelly J. N., Kouchinsky A., Gill B. C., Mansson S. F. and Bizzarro M. (2017) Reorganisation of Earth's biogeochemical cycles briefly oxygenated the oceans 520 Myr ago. *Geochem. Perspect. Lett.* **3**, 210–220.

DeCarlo T. M., Gaetani G. A., Holcomb M. and Cohen A. L. (2015) Experimental determination of factors controlling U/Ca of aragonite precipitated from seawater: implications for interpreting coral skeleton. *Geochim. Cosmochim. Acta* **162**, 151–165.

Diaz M. R., Van Norstrand J. D., Eberli G. P., Piggot A. M., Zhou J. and Klaus J. S. (2014) Functional gene diversity of oolitic sands from Great Bahama Bank. *Geobiology* **12**, 231–249.

Diaz M. R., Swart P. K., Eberli G. P., Oehlert A. M., Devlin Q., Saeid A. and Altabet M. A. (2015) Geochemical evidence of microbial activity within ooids. *Sedimentology* **62**, 2090–2112.

Diaz M. R., Eberli G. P., Blackwelder P., Phillips B. and Swart P. K. (2017) Microbially mediated organomineralization in the formation of ooids. *Geology* **45**, 771–774.

Duguid S. M. A., Kyser T. K., James N. P. and Rankey E. C. (2010) Microbes and ooids. *J. Sediment. Res.* **80**, 236–251.

Dunk R. M., Mills R. A. and Jenkins W. J. (2002) A reevaluation of the oceanic uranium budget for the Holocene. *Chem. Geol.* **190**, 45–67.

Elrick M., Polyak V., Algeo T. J., Romaniello S. J., Asmerom Y., Herrmann A. D., Anbar A. D., Zhao L. and Chen Z. (2017) Global-ocean redox variation during the middle-late Permian through Early Triassic based on uranium isotope and Th/U trends of marine carbonates. *Geology* **45**, 163–166.

Endrizzi F. and Rao L. (2014) Chemical speciation of Uranium(VI) in marine environments: Complexation of calcium and magnesium ions with $[(UO_2)(CO_3)_3]^{4-}$ and the effect on the extraction of Uranium from seawater. *Chem. Eur. J.* **20**, 14499–14506.

Felis T., Suzuki A., Kuhnert H., Dima M., Lohmann G. and Kawahata H. (2009) Subtropical coral reveals abrupt early twentieth-century freshening in the western North Pacific Ocean. *Geology* **37**, 527–530.

Gabitov R. I., Gaetani G. A., Watson E. B., Cohen A. L. and Ehrlich H. L. (2008) Experimental determination of growth rate effect on U^{6+} and Mg^{2+} partitioning between aragonite and fluid at elevated U^{6+} concentration. *Geochim. Cosmochim. Acta* **72**, 4058–4068.

Gaetani A. A., Cohen A. L., Wang Z. and Crusius J. (2011) Rayleigh-based, multi-element coral thermometry: a biomineralization approach to developing climate proxies. *Geochim. Cosmochim. Acta* **75**, 1920–1932.

Gagnon A. C., Adkins J. F., Fernandez D. P. and Robinson L. F. (2007) Sr/Ca and Mg/Ca vital effects correlated with skeletal architecture in a scleractinian deep-sea coral and the role of Rayleigh fractionation. *Earth Planet. Sci. Lett.* **261**, 280–295.

Gagnon A. C., Adkins J. F. and Erez J. (2012) Seawater transport during coral biomineralization. *Earth Planet. Sci. Lett.* **329–330**, 150–161.

Galloway S. B., Work T. M., Bochsler V. S., Harley R. A., Kramarsky-Winter E., McLaughlin S. M. (2007) Coral disease and health workshop: coral histopathology II. NOAA Technical Memorandum NOSNCCOS 56 and NOAA Technical Memorandum CRCP 4. National Oceanic and Atmospheric Administration, Silver Spring, MD. pp 10–11.

Gattuso J. P., Pichon M., Delesalle B. and Frankignoulle M. (1993) Community metabolism and air-sea CO_2 fluxes in a coral reef ecosystem (Moorea, French Polynesia). *Mar. Ecol. Prog. Ser.* **96**, 259–267.

Gattuso J. P., Pichon M., Delesalle B., Canon C. and Frankignoulle M. (1996) Carbon fluxes in coral reefs: I. Lagrangian measurement of community metabolism and resulting air-sea CO_2 disequilibrium. *Mar. Ecol. Prog. Ser.* **145**, 109–121.

Gilbert P. U. P. A. and Wilt F. H. (2011) Molecular aspects of biominieralization of the Echindoderm Endoskeleton. In *Molecular Biomineralization* (ed. W. Müller). Springer, Berlin-Heidelberg, pp. 199–223.

Gorzelak P., Stolarski J., Dubois P., Kopp C. and Meibom A. (2011) ^{26}Mg labeling of the sea urchin regenerating spine: insights into echinoderm biomineralization process. *J. Strt. Biol.* **176**, 119–126.

Harris P. M. (2010) Delineating and quantifying depositional facies patterns in carbonate reservoirs: insights from modern analogs. *AAPG Bull.* **94**, 61–68.

Henehan W. J., Foster G. L., Bostock H., Greenop R., Marshall B. J. and Wilson P. A. (2016) A new boron isotope-pH calibration for *Orbulina universa*, with implications for understanding and accounting for 'vital effects'. *Earth Planet. Sci. Lett.* **454**, 282–292.

Inoue M., Suwa R., Suzuki A., Sakai K. and Kawahata H. (2011) Effects of seawater pH on growth and skeletal U/Ca ratios of *Acropora digitifera* coral polyps. *Geophy. Res. Lett.* **38**, L12809.

Jodrey L. H. (1953) Studies on shell formation. 3. Measurement of calcium deposition in shell and calcium turnover in mantle tissue using the mantle-shell preparation and Ca^{45}. *Biol. Bull.* **104**, 398–407.

John S. G. and Adkins J. F. (2010) Analysis of dissolved iron isotopes in seawater. *Mari. Chem.* **119**, 65–76.

Jost A. B., Bachan A., Schootbrugge B. v. d., Lau K. V., Weaver K. L., Maher K. and Payne J. L. (2017) Uranium isotope evidence for an expansion of marine anoxia during the end-Triassic extinction. *Geochem. Geophys. Geosyst.* **18**, 3093–3108.

Keul N., Langer G., de Nooijer L. J., Nehrke G., Reichart G. J. and Bijma J. (2013) Incorporation of uranium in benthic foraminiferal calcite reflects seawater carbonate ion concentration. *Geochem. Geophys. Geosyst.* **14**, 102–111.

Krumbein W. E. (1979) Calcification by bacteria and algae. In *Biogeochemical Cycling of Mineral-Forming Elements* (eds. P. A. Trudinger and D. J. Swaine). Elsevier, Amsterdam, pp. 47–68.

Lau K. V., Maher K., Altiner D., Kelley B. M., Kump L. R., Lehrmann D. J., Silver-Tamayo J. C., Weaver K. L., Yu M. and Payne J. L. (2016) Marine anoxia and delayed Earth system recovery after the end-Permian extinction. *Proc. Natl. Acad. Sci.* **113**, 2360–2365.

Lau K. V., Macdonald F. A., Maher K. and Payne J. L. (2017) Uranium isotope evidence for temporary ocean oxygenation in the aftermath of the Sturtian Snowball Earth. *Earth Planet. Sci. Lett.* **458**, 282–292.

Mackenzie F. T. and Morse J. W. (1992) Sedimentary carbonates through Phanerozoic time. *Geochim. Cosmochim. Acta* **56**, 3281–3295.

Min G. R., Edwards R. L., Taylor F. W., Recy J., Gallup C. D. and Beck J. W. (1995) Annual cycles of U/Ca in coral skeletons and U/Ca thermometry. *Geochim. Cosmochim. Acta* **59**, 2025–2042.

Nakano E., Okazaki K. and Iwamatsu T. (1963) Accumulation of radioactive calcium in larvae of the sea urchin *pseudocentrotus depressus*. *Biol. Bull.* **125**, 125–132.

Ohde S. and van Woesik R. (1999) Carbon dioxide flux and metabolic processes of a coral reef, Okinawa. *Bull. Mar. Sci.* **65**, 559–576.

Ortegón-Aznar I., Chuc-Contreras A. and Collado-Vides L. (2017) Calcareous green algae standing stock in a tropical sedimentary coast. *J. Appl. Phycol.* **29**, 2685–2693.

Pretet C., Samankassou E., Felis T., Reynaud S., Böhm F., Eisenhauer A., Ferrier-Pagès C., Gattuso J. P. and Camoin G. (2013) Constraining calcium isotope fractionation ($\delta^{44/40}$Ca) in modern and fossil scleractinian coral skeleton. *Chem. Geol.* **340**, 49–58.

Romaniello S. J., Herrmann A. D. and Anbar A. D. (2013) Uranium concentrations and ^{238}U/^{235}U isotope ratios in modern carbonates from the Bahamas: assessing a novel paleoredox proxy. *Chem. Geol.* **362**, 305–316.

Shen G. T. and Dunbar R. B. (1995) Environmental controls on uranium in reef corals. *Geochim. Cosmochim. Acta* **59**, 2009–2024.

Shields G. and Veizer J. (2002) Precambrian marine carbonate isotope database: Version 1.1. *Geochem. Geophys. Geosyst.* **3**, 1–12.

Song H., Song H., Algeo T. J., Tong J., Romaniello S. J., Zhu Y., Chu D., Gong Y. and Anbar A. D. (2017) Uranium and carbon isotopes document global-ocean redox productivity relationships linked to cooling during the Frasnian-Famennian mass extinction. *Geology* **45**, 887–890.

Stirling C. H., Andersen M. B., Potter E. K. and Halliday A. N. (2007) Low-temperature isotopic fractionation of uranium. *Earth Planet. Sci. Lett.* **264**, 208–225.

Tambutté T., Tambutté S., Segonds N., Zoccola D., Venn A., Erez J. and Allemand D. (2012) Calcein labelling and electrophysiology: Insights on coral tissue permeability and calcification. *Proc. R. Soc. London Ser. B* **219**, 19–27.

Tissot F. L. H. and Dauphas N. (2015) Uranium isotopic compositions of the crust and ocean: age corrections, U budget and global extent of modern anoxia. *Geochim. Cosmochim. Acta* **167**, 113–143.

Verbruggen A., Alonso-Munoz A., Eykens R., Kehoe F., Kuhen H., Richter S. and Arbegbe Y. (2008) Preparation and certification of IRMM-3636, IRMM-3636a and IRMM-3636b. *OPOCE*, 24.

Wang X. L., Planavsky N. J., Hull P. M., Tripati A. E., Zou H. J. and Heneha M. (2016) Chromium isotopic composition of core-top planktonic foraminifera. *Geobiology*. https://doi.org/10.1111/gbi.12198.

Weyer S., Anbar A. D., Gerdes A., Gordon G. W., Algeo T. J. and Boyle E. A. (2008) Natural fractionation of ^{238}U/^{235}U. *Geochim. Cosmochim. Acta* **72**, 345–359.

Wizemann A., Meyer F. W. and Westphal H. (2014) A new model for the calcification of the green macro-alga *Halimeda opuntia* (Lamouroux). *Croal Reefs* **22**, 951–964.

Wray J. L. (1977) Calcareous Algae—Developments in Paleontology and Stratigraphy, Volume 4. Elsevier, Amsterdam.

Zhang F., Algeo T. J., Romaniello S. J., Cui Y., Zhao L., Chen Z. and Anbar A. D. (2018a) Congruent Permian-Triassic δ^{238}U records at Panthalassic and Tethyan sites: confirmation of global-oceanic anoxia and validation of the U-isotope paleoredox proxy. *Geolgoy* **46**, 327–330.

Zhang F., Romaniello S. J., Algeo T. J., Lau K. V., Clapham M. E., Richoz S., Herrmann A. D., Smith H., Horacek M. and Anbar A. D. (2018b) Multiple episodes of extensive marine anoxia linked to global warming and continental weathering following the latest Permian mass extinction. *Sci. Adv.* **4**, 61602921.

Associate editor: Stefan Weyer